Slumped glass foils as substrate for adjustable X-ray optics

Bianca Salmaso, Stefano Basso, Marta Civitani, Mauro Ghigo, Joanna Hołyszko, Carlo Pelliciari, Daniele Spiga, Gabriele Vecchi, Giovanni Pareschi

INAF/Brera Astronomical Observatory, Via E. Bianchi 46, 23807 Merate, ITALY

ABSTRACT

Thin glass modular mirrors are a viable solution to build future X-ray telescopes with high angular resolution and large collecting area. In our laboratories, we shape thin glass foils by hot slumping and we apply pressure to assist the replication of a cylindrical mould figure; this technology is coupled with an integration process able to damp low frequency errors and produces optics in the Wolter I configuration, typical for the X-ray telescopes. From the point of view of the hot slumping process, the efforts were focused in reducing low-, mid- and high- frequency errors of the formed Eagle glass foils. Some of our slumped glass foils were used for the development of active X-ray optics, where piezoelectric actuators are used to correct the slumped glass foil deviations from the ideal shape. In particular, they were used for the Adjustable X-raY optics for astrOnoMy project (AXYOM) developed in Italy, and the X-ray Surveyor mission, as developed at the Smithsonian Astrophysical Observatory / Center for Astrophysics (SAO/CfA) in USA. In this paper we describe the optimisation of the hot slumping process, comparing the results with the requirements of the considered active optics projects. Finally, since the present configuration of the Pennsylvania State University (PSU) coating equipment is limited to 100×100 mm^2, the slumped glass foils used for the SAO project were cut from 200×200 mm^2 to 100×100 mm^2, and a low-frequency change was observed. A characterisation of the profile change upon cutting is presented.

Keywords: Slumped Glass Optics, adjustable optics, hot slumping, thin glass mirrors, Zerodur K20, Eagle XG, glass cutting.

1. INTRODUCTION

The next generation of the X-ray telescopes will have very high angular resolution and large collecting area. Thin glass foils, shaped by hot slumping, are considered good candidates for the substrates. Great efforts are on going world wide to minimise low-, mid- and high-frequency errors of the glass mirrors made by this replication technique. To go beyond the performance of a replica process, one possible approach is to use active devices for the figure correction of the slumped glass foils. Due to the tight nesting typical of an X-ray telescope, X-ray active optics cannot use normal actuators on the back of the mirrors, as typically done in optical astronomy. On the contrary, the use of piezoelectric elements acting tangentially, i.e., exerting a strain in a direction parallel to the surface on the rear of the glass foil, enable the changes of the local curvature of the mirror to correct profile errors. There are two competing ways of realising active optics for astronomical applications. The first method is to have individual piezoelectric actuators tiled and bonded onto the back of the mirror. The second method is to create a complete, single layer, coating of thin piezoelectric material on the reverse of the glass and print the electrode pattern required onto the material to actuate the individual areas. The two approaches are adopted in the projects hereafter described.

Adjustable X-raY optics for astrOnoMy (AXYOM) (Italy) is a PRIN-TECNO-INAF 2012 project led by INAF-OAB, and performed in collaboration with INAF-OAPA (Osservatorio Astronomico di Palermo) and Università di Palermo.[1,2] It is aimed at developing the actuation, with piezoelectric components commercially available, of thin slumped glass X-ray mirrors, integrated with glass ribs with the process developed at INAF-OAB.[3] The innovation therefore consists on the possibility to combine ribs and piezoelectric elements, glued in the space within the ribs, to correct some of the shape errors of the slumped glass foils. Another innovation

---

of the project is to test the possibility of optimising the mirror shape directly in X-ray illumination, in intra-focal setup.[4] The mirror substrates adopted for this project are Eagle glass foils slumped at INAF-OAB. The integration with ribs corrects the shape of the glass foils for residual forming errors, in the low-frequency range, to an extent that improves as the nearest rib is approached. Therefore the maximum error is expected to be in between two adjacent ribs. At these position, piezoelectric elements are glued to perform the correction of the errors in the centimetre scale. To contact the piezoelectric elements, a lithographic process has been developed which prints the conductive tracks on the back side of the cylindrical glass.[5] Moreover, a modular multichannel electronic driver was designed and built to drive simultaneously up to 16 actuators with a very low power consumption.[5] The results obtained on this project are presented in detail in another paper.[2]

The X-ray Surveyor mission was presented by NASA,[6] in January 2015, in response to the 2020 Decadal Survey. The goal is to look beyond Chandra, therefore combining comparable angular resolution with greatly increased photon throughput. To maintain sub-arcsec resolution over a large effective area, a number of efforts are on going. These include both active (piezoelectric actuator deposition[7] and magnetorestrictive optics[8]) and passive (differential deposition,[9] ion implantation,[10] low stress single crystal silicon mirrors,[11] and direct polishing[12, 13]) methods to achieve the desired imaging. Active X-ray optics for the X-ray Surveyor missions are developed at SAO. Motivated initially by the Generation-X mission concept,[14] SAO approach was to deposit a piezoelectric film (PZT, lead zirconate titanate), while in parallel the SMART-X consortium, UK based, was gluing shaped piezoelectric PZT pads to the back of the mirror.[15] More recently, SAO continued the work on the deposition process for the SMART-X mission concept.[16] Nowadays,[6] this approach is one of the possible for the X-ray Surveyor mission concept. The PZT ceramic actuator arrays are developed at Pennsylvania State University (PSU).[17] The advantages of this method include the fact that no print-through is created as the material is deposited directly onto the mirror without the need of bonding. The main disadvantage is that the piezoelectric material requires annealing, and therefore also the mirror has to undergo a thermal cycle which could result in irreversible degradation of the mirror shape. In order to solve this issue, PSU had developed a PZT deposition process with a crystallization temperature lower than the initial ~ 700 ℃ used in micro-electromechanical (MEMS) systems: this temperature could be set to 550 ℃. On the other side, SAO defined Schott D263 (the glass used for the NuSTAR telescope) not suitable due to its annealing temperature (557 ℃) too close to the one necessary for the PZT crystallisation. The Corning Eagle glass instead (T_{anneal}=722 ℃) was defined compatible with the PZT process.[18]

In 2013, we started developing a hot slumping process assisted by pressure for the Corning Eagle glass. The process was initially developed with Schott D263 glass foils, combined with a Fused Silica slumping mould and a Cr+Pt detaching layer.[19] Due to the degradation of the detaching layer after few slumping cycles, the mould material was changed to Zerodur K20 and the glass was changed from D263 to AF32, both produced by Schott, for the better quality obtained in the slumped glass foils, owing the better coupling of Coefficient of Thermal Expansion ($CTE_{K20} = 2.0 \ 10^{-6}/K$, $CTE_{D263} = 7.2 \ 10^{-6}/K$, $CTE_{AF32} = 3.2 \ 10^{-6}/K$). Finally the glass was changed to Corning Eagle glass which have a CTE very similar to the one of AF32 ($CTE_{Eagle} = 3.17 \ 10^{-6}/K$): one of the reason was the starting of the collaboration with SAO.[20] Actually our process was developed for the IXO mission, and some parameters selected for the development of the process were kept also during the following research. In particular, we slump 0.4 mm thin glass foils with cylindrical shape and radius of curvature of 1 m; we cut them to 200×200 mm^2, and we integrate the slumped glass foils with an integration process able to damp low frequency errors and produce optics in the Wolter I configuration, for 20 m focal length and 0.7 deg incidence angle.[3] Owing the cylindrical shape, our slumped glass foils cannot be directly considered as substrates for the X-ray Surveyor optics; instead they were considered by SAO for the active pre-deterministic figure correction of curved glass,[21] the follow up of a similar test on flat glass.[22]

The aim of this paper is to present the results of our hot slumping process, considering the application of our substrates to active X-ray optics. The reference tolerance are considered the ones of the X-ray Surveyor mission, which are the tightest ever defined:

1. high frequency errors have to be maintained as the ones of the glass foil prior the slumping, as they cannot be corrected by the active elements: therefore the rms has to be kept below 4 Å;

2. mid frequency errors can be corrected only for spatial wavelength larger than the piezo-element size; the tolerance was therefore set to rms [1-10 mm] $\leq$ 1 nm;

3. for what concern the low frequency errors, the peak to valley (PV) should be maintained below 1-2 μm to reach the 0.5 arcsec resolution requirement; anyway for the deterministic figure correction test, no stringent requirement was given.

The following sections describe the work performed at OAB to go towards these tolerances on the slumped glass foils. Section 2 describes the slumping setup, our thermal cycle, the measurements of the thermal gradients inside the slumping environment, the pressure control system, the result obtained with the pressure controlled in closed or open loop, and finally the trend in the reduction of the low- mid- and high- frequency errors of the slumped glass foil. Section 3 presents the approach followed for the characterisation of the mid-frequency errors, with special care to the understanding of the errors in the 1 $\div$10 mm range, as this range cannot be corrected nor by the AXYOM or the SAO active concept. Finally, Section 4 presents the result obtained upon cutting the slumped glass foils from 200 $\times$ 200 mm^2 to 100 $\times$ 100 mm^2, as required by the deposition chamber present at PSU.

2. THE HOT SLUMPING AT INAF-OAB

At INAF-OAB, we have developed a direct hot slumping approach, in which a thin glass foil is positioned over a convex mould, whose shape has to be replicated in negative.[19] The mould and the glass are closed inside a muffle, and positioned in a furnace where the glass foil is curved with a proper thermal cycle and with the assistance of pressure. The glass is slumped with dimension larger than the mould, as it also acts as membrane to divide the muffle chamber in two parts: the pressure is exerted by vacuum suction from the lower part (INAF patent TO2013A000687, 12/08/2013). At the end of the process, the slumped glass has to be trimmed from the original dimension 340 $\times$ 340 mm^2 to the final of 200 $\times$ 200 mm^2.

2.1 The furnace at INAF-OAB

All thermal slumping cycles to produce cylindrical glass foils were conducted in a thermal furnace purchased from Teknokilns and installed at INAF-OAB. The furnace can reach a maximum temperature of 950 ℃, using five different heating zones, each one equipped with its own K-type thermocouple. A sector consists of the lateral electrical resistors and the other sectors are represented by the upper and lower resistors, both composed by two separate heating elements, a central one and a lateral one following the perimeter of the oven. The heating zones can be switched on and off separately, depending on the thermal cycle adopted.

2.2 The muffle: thin-open or thick-close cover

The muffle, made of AISI 310 stainless steel, is placed in the middle of the furnace, to contain the mould and the glass foil. It enables the pressure application by using the glass foil as a membrane to divide the muffle in two chambers (Fig. 3-left). It also has the effect to create a clean and uniform environment for the slumping. Clearly, a closed muffle is preferable to minimise the thermal gradients (Fig. 1-right). Nevertheless, the open muffle configuration (Fig. 1-left) was used for a long time, during the development of the process, to monitor the glass during the slumping with the interference fringes between the glass and the mould surfaces.[20] A thin open shield is used in this configuration. Among the glass foils described in this paper, the ones of Section 3, slumped at earlier times, were produced with the thin-open configuration, while the ones described in Section 2.6 and 2.7 adopted the thick-closed configuration.

2.3 The thermal cycle

A thermal cycle for slumping is typically divided into a heating time, to reach a maximum temperature called *slumping temperature* or *soaking temperature* (somewhat higher than the annealing temperature); a holding time at the soaking temperature, a cooling time at controlled speed down to the strain temperature, and finally a faster cooling time down to room temperature. The thermal cycle has to be set in such a way to reduce the temperature gradients present in the mould, especially during the cooling down phase, when the glass foil freezes its shape. In the cooling phase however, the edges of the mould cool down faster than
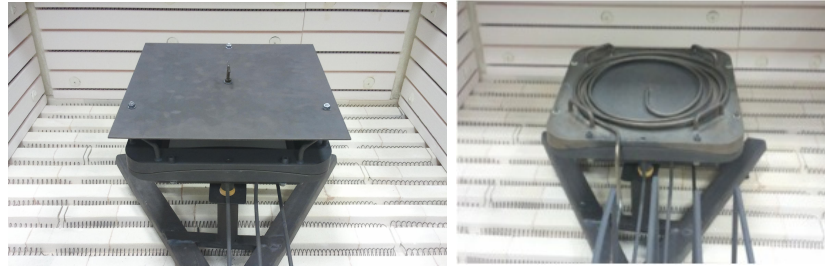
Figure 1. : *The muffle inside the large furnace. Left: open configuration to enable the interference fringes recording; only a shield is present. The glass is clamped with a cylindrical frame, visible under the thin shield. Right: the muffle is closed with a cylindrical cover.*

its centre. Finite element analysis (FEA) was previously performed[23] to define the best use of the different heating zones during the thermal cycle: the central top and bottom resistors are used during the heating and holding time, while the lateral resistors are used during the cooling time, below the annealing temperature. Table 1 reports the thermal cycle, as optimised during the research, and used for the glass foils described in Section 2.6 with the exception of the one described in Section 2.7, where a new thermal cycle was adopted to reduce the mould roughness replication. Compared to the previous works,[23] the soaking time was set 2 h longer to reduce the sag error, the cooling cycle was divided into two steps of different cooling rate, before and after the strain temperature, and the cooling rate was lowered from the original 9.6 ℃/h to 2.5 ℃/h in the region from the annealing ($T_{anneal-Eagle}$=722 ℃) to the strain temperature ($T_{strain-Eagle}$=669 ℃). The latter was found to reduce the mid frequency errors, as in this region the cooling ramp has to be sufficiently slow to let the glass foil to relax and release internal stresses[24, 25] .

Table 1. : *The thermal cycle, optimised to minimise low- and mid- frequency errors.*

Step	Temperature [℃]	Time	Speed [℃/h]	Heating zone ON
1	to 750	11 h	66.4	central top and bottom
2	@ 750	4 h		central top and bottom
3	to 722	4 h	7	central top and bottom
4	@ 722	2 h		central top and bottom
5	@ 722	10 min		lateral
6	to 670	21 h	2.5	lateral
7	to 600	8 h	8.8	lateral
free cooling				

2.4 Temperature monitoring inside the muffle

The furnace is equipped with five internal thermocouples, positioned very close to the oven resistors. Actually, the temperature inside the muffle can be different, and gradients among the different parts of the mould can be present. To monitor the temperature at the level of the cylindrical mould, the cylindrical muffle was modified to house the heads of two thermocouples, and measure the temperature of the mould at the bottom and lateral sides (Fig. 2). The thermocouples were calibrated to give the same temperature value when being at the same temperature.

Fig. 2-right shows the temperatures measured with the closed muffle configuration and the thermal cycle of Table 1, as used for the glass foils of Section 2.6 and 2.7. The maximum temperature gradient inside the muffle is ∼ 2-3 ℃, during the soaking time and the first part of the cooling time, until the reaching of the annealing temperature. During this period, the lateral part of the mould is colder than the bottom part, consistently with the fact that the driving resistors are the top and bottom ones. In the cooling phase, below the annealing temperature, the driving resistors is set to be the lateral one, to heat the lateral side of the
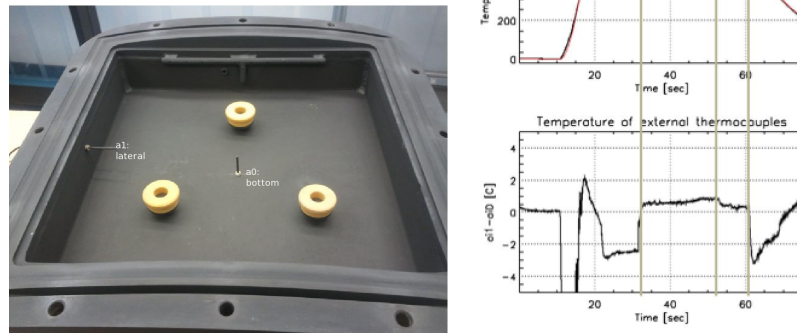
Figure 2. : *Left: the external thermocouple heads, entering the muffle, to measure the temperature of the bottom (ai0) of lateral part (ai1) of the mould. Right-top: the thermal cycle of a glass foil slumped with a closed muffle configuration (Fig. 1-right), with the cycle described in Table 1. Right-bottom: the temperature difference of ai0 and ai1 shows that the bottom and lateral part of the mould are almost at the same temperature in the cooling region from 722 to 600 ℃.*

mould while this would cool faster than the core part. Fig. 2-right shows that the gradients are less than 1 ℃ in the critical cooling region from 722 to 670 ℃, when thes shape of the glass foil is frozen,[20,25] and maintained to this level down to 600 ℃.

2.5 The pressure control system: open and closed loop

To force the glass foil to come in contact with the mould, a differential pressure is applied in the two chambers of the muffle. A rotative vacuum pump is connected to the lower chamber of the muffle and the vacuum pressure is controlled, either in open or closed-loop system (Fig. 3). A capacitance-based manometer (Baratron valve 626B) is inserted in the air flow: this system measures changes of pressure/vacuum as changes in capacitance between the sensor's diaphragm and an adjacent electrode disk. It provides a 0-10 VDC analog output, linear with pressure, with a 0.25% accuracy, fed to a pressure control module from MKS (MKS-205E): it can keep the desired pressure constant (closed-loop configuration), by feedback to the control valve MKS-248, thus enabling a controlled gas flow.
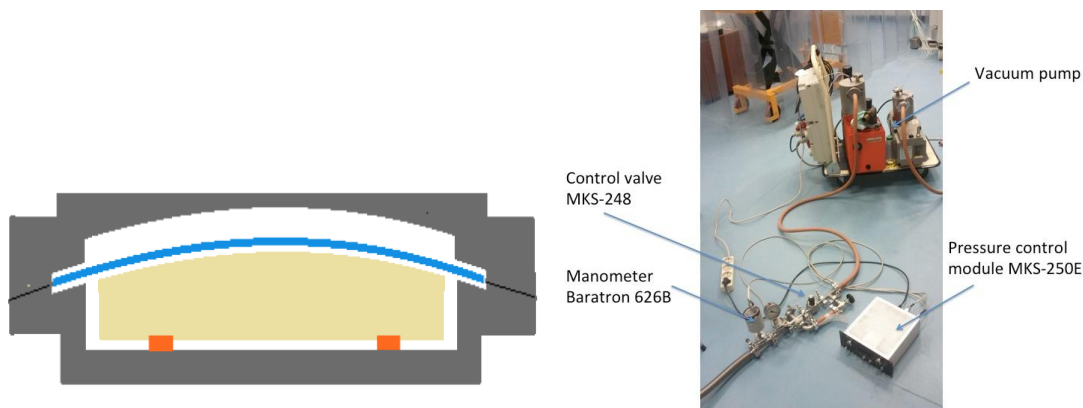

Figure 3. : *Left: A flat glass foil is positioned over a cylindrical mould, inside a stainless steel muffle. With this setup, the glass itself can act as a membrane that allows the pressure application. Right: The pressure control system.*

Recently, the control module 205E has been connected to the 9205 module from National Instrument, and the external thermocouples shown in Fig. 2-left to the NI-9211 module, in order to perform the temperature and pressure data acquisition with a DaQ system. It was recognised that, in order to have a real closed

loop configuration, the control valve MKS-248 should have a periodical maintenance, as dirt inside the valve, deposited after several slumpings, would not enable the closed loop to correctly operate. Anyway, it was also recognised that an open loop configuration would allow a better relaxation of the glass, especially from the low-frequency errors view point. This is visible from the LTP profile comparison of a glass foil slumped in closed loop configuration after a proper maintenance of the valve (E46 glass code in Fig. 4) and a glass foil slumped in open loop configuration (E59 glass code in Fig. 6). At the moment, the open loop configuration is believed to be the more appropriate for our hot slumping process.

2.6 The results with different pressure controls

We here present the results obtained with different pressure control system: the goal was to determine the pressure condition that minimise the errors on the slumped glass foils. Fig. 4 show the result obtained on a closed loop configuration with a pressure value of 50 g/cm^2, applied from the soaking temperature. From Fig. 4-centre, it can be noted that the relatively high level of pressure, constantly maintained, triggers an increase in the low-frequency error, compared to the other process conditions (Fig.s 5-centre and 6-centre). To evaluate the mid-frequency error content, we have computed the rms in the region from 1 to 10 mm from the five LTP scans after the subtraction of the 8th order best fit polynomial, giving a value of 9.6 nm for the E46 foil.
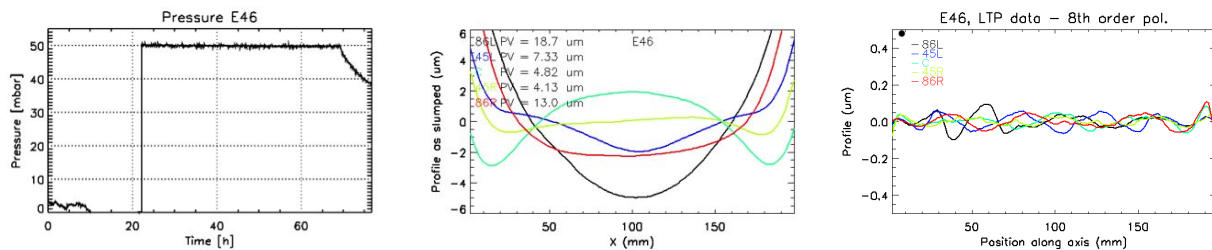

Figure 4. : E46 glass foil. Left: the applied pressure in closed loop. Center: raw LTP profiles. Right: LTP profile after removing the best fit 8th order polynomial, giving rms[1-10mm] = 9.6 nm.

Some glass foils were slumped with the pressure in closed loop, but at reduced value. A constant pressure of 30 g/cm^2 could not be applied, as it was found to trigger air bubbles entrapping between the glass and the mould. A pressure of 50 g/cm^2 was therefore applied for the first hour after the reaching of the soaking temperature: this time was experimentally defined as sufficient to enable the disappearing of the air bubbles; after that, a pressure of 30 g/cm^2 was maintained in closed loop until the end of the process (Fig. 5). While giving good results in terms of decreased low- and mid-frequency errors, this configuration was found not stable from glass to glass.
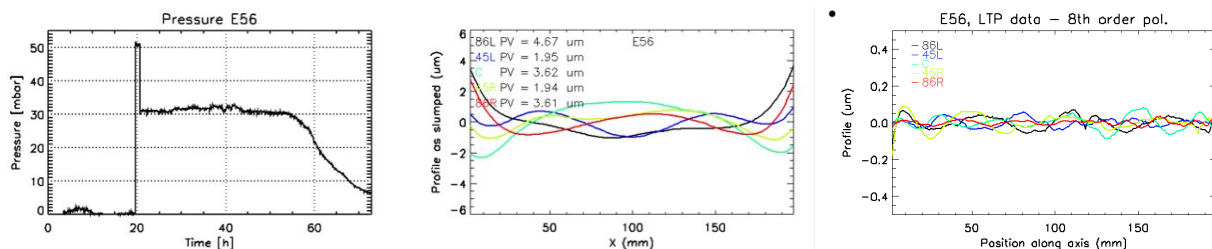

Figure 5. : E56 glass foil. Left: the applied pressure in closed loop. Center: raw LTP profiles. Right: LTP profile after removing the best fit 8th order polynomial, giving rms[1-10mm] = 8.7 nm.

Actually it was recognised that the closed loop could not be maintained properly after few slumping cycles, and a periodical cleaning was necessary on the valve MKS-248. Moreover, it was proved with the slumping of 10 glass foils in open loop configuration,[24] that the open loop setting could efficiently correct both low- and mid-frequency errors, giving stable results from glass to glass. Fig. 6 shows the pressure

setting and the LTP profiles on one of them. For this foil the rms computed in the range 1 to 10 mm, after removing the 8th order best fit polynomial is 5.3 nm.
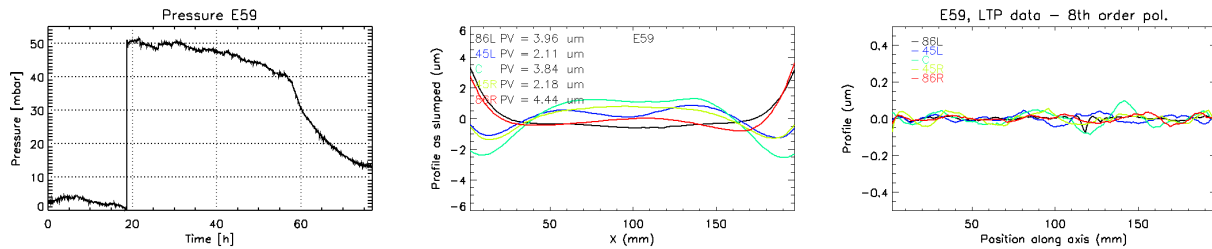

Figure 6. : E59 glass foil. Left: the applied pressure in open loop. Center: raw LTP profiles. Right: LTP profile after removing the best fit 8th order polynomial, giving rms[1-10mm] = 5.3 nm.

The rms computed from the 5 LTP scans, after removing the 8th order best fit polynomial, is still much higher than the given tolerance of 1 nm, even in the best case of the E59 foil. Actually this is computed for foils of 200×200 mm^2. Anyway, a full discussion on the evaluation of the mid-frequency errors will be presented in Section 3.

2.7 The new thermal cycle to reduce the high-frequency errors

The pressure assistance, although essential to reduce the errors contribution in the centimeter spatial wavelength range, was leading to a partial replication of the mould micro-roughness.[26,27] Attempts to reduce the roughness replication, by reducing the pressure value below our standard value of 50 g/cm^2 for at least 1 h, were leading to an increase in the mid-frequency errors[27] or to air bubble entrapping, as described in the previous section. A different approach was therefore developed. It was already described in another paper,[24] but we summarise also here the results for completeness. A new thermal cycle with a zero soaking time was used, while the pressure was kept at 50 g/cm^2 in open loop: Fig. 7 compares the old and new thermal cycles, and the result obtained in terms of PSD from roughness data. The micro-roughness is reduced in all the spatial wavelength range, while the contribution from the mid frequency errors is substantially unchanged, as proven in another paper,[24] owing the pressure value of 50 g/cm^2 in both cases.
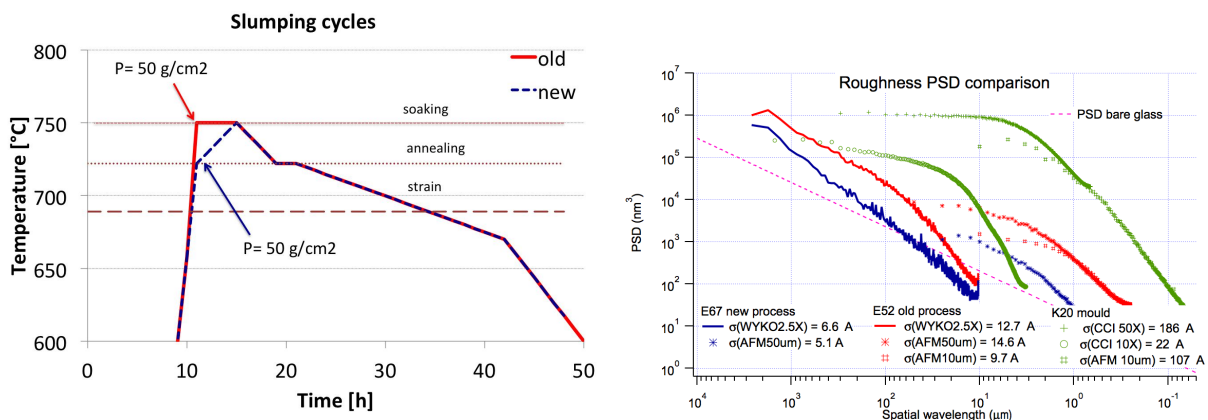

Figure 7. : Left: thermal cycles comparison: the blue dashed line represents the new thermal cycle that reduce the mould roughness replication; the red solid line represents the old thermal cycle. Right: PSD from roughness data for one glass foil slumped with the new process (glass code E67, blue line), and one slumped with the old process (glass code E52, red line). The K20 mould roughness (green line) is reported for comparison.

2.8 The decreasing trend for the low- mid- and high-frequency errors

Several process changes were introduced during our research in order to minimise the low- mid- and high-frequency errors, such as optimisation of the mould height inside the muffle, procurement of a Zerodur

K20 with improved surface quality, closing of the muffle to reduce the thermal gradients, reduction of the cooling rate, introduction of cleaning protocols.[20, 24, 25] The results obtained in a three years project can be summarised by the trends presented in Fig. 8, where three figures of merit were adopted to measure the improvements in the low- mid- and high-frequency range. Actually these figures of merit are relevant for the integration approach with ribs developed at INAF-OAB, and therefore can be considered appropriate for the AXYOM project, where both ribs and active elements are considered, but not for the X-ray surveyor case, where no ribs are present in the integration scheme. Nevertheless they show the great improvement obtained through the years to reduce the deviation from nominal of the slumped glass figure and roughness. A brief discussion about these figures for the X-ray Surveyor case is presented hereafter:

- the PV of the overall foil should be considered for the final application of reaching the 0.5 arcsec angular resolution. Fig. 8-left shows the PV of the central scan only. For the overall foil we are still very far from the 1-2 μm requirement for the X-ray Surveyor, but we remind that the goal of this phase was to use the glass foils slumped at OAB for the deterministic figure correction test, where no strict requirement is present on the foil PV;

- since the integration with ribs is damping low frequency errors, the HEW computed after integration has been considered a good figure of merit for the evaluation of the mid-frequency errors, when such integration is applied, for the IXO/ATHENA application as developed at INAF-OAB. For the X-ray Surveyor case, a more detailed discussion about the evaluation of mid-frequency errors in given in Section 3;

- the WYKO roughness is a good parameter also for the X-ray Surveyor case to evaluate the contribution of the high frequency errors, as they cannot be correct by any integration approach. The reached value of 6-7 $\mathring{A}$ is now very close to the one of the bare new glass. For further improvement, a K20 mould with better surface quality than the one used at the moment should be adopted; this higher-level polishing seems to be feasible.[24]
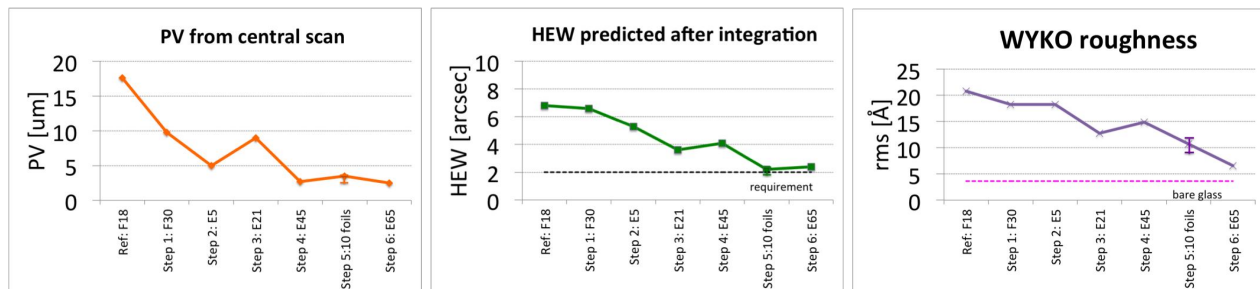

Figure 8. : *Trend of three figures of merit selected to describe the reduction of the low- mid- and high- frequency errors of the glass foils slumped to cylindrical shape and integrated with ribs to Wolter I shape, for the IXO/ATHENA application as developed at INAF-OAB. Left: PV of the central LTP scan, the most critical as the less corrected during the integration with ribs. Center: HEW values expected from the LTP slumped glass profiles, obtained with physical optics[28] in single reflection after the simulation of a perfect integration. Right: roughness from the WYKO data.*

3. EVALUATION OF THE MID-FREQUENCY ERRORS ON THE GLASS FOILS SLUMPED AT INAF-OAB

3.1 First test: cross check characterisation at INAF-OAB and SAO/CfA

To determine the quality of our slumped glass foils in the range 1 ÷10 mm, very critical as this range cannot be corrected nor by the AXYOM or the SAO active concept, checks were performed at the beginning of the collaboration with the SAO group. A glass foil (code E21), slumped on a K20 mould with good surface quality was selected. The CUP[29] map and the LTP characterisation are shown in Fig. 9. Actually, at the time this glass was produced, the slumping process was still not including three main process modifications, described also in a previous paper:[20]

1. proper cleaning protocols on the mould side: the effect is visible on the bottom corners of the CUP map of Fig. 9-left, where spots are present due to contaminations on the mould side, not properly cleaned, and replicated on consecutive slumped glass foils.

2. optimisation of the mould height inside the muffle: the effect is evident in the large peak to valley of the LTP profiles (Fig. 9-right);

3. cooling rate reduction[20, 24, 25] in the region around the strain temperature: cool-rate$_{E21}$ = 9.4 ℃/h, cool-rate$_{E32}$ = 4 ℃/h, cool-rate$_{optimised}$ = 2.5 ℃/h.
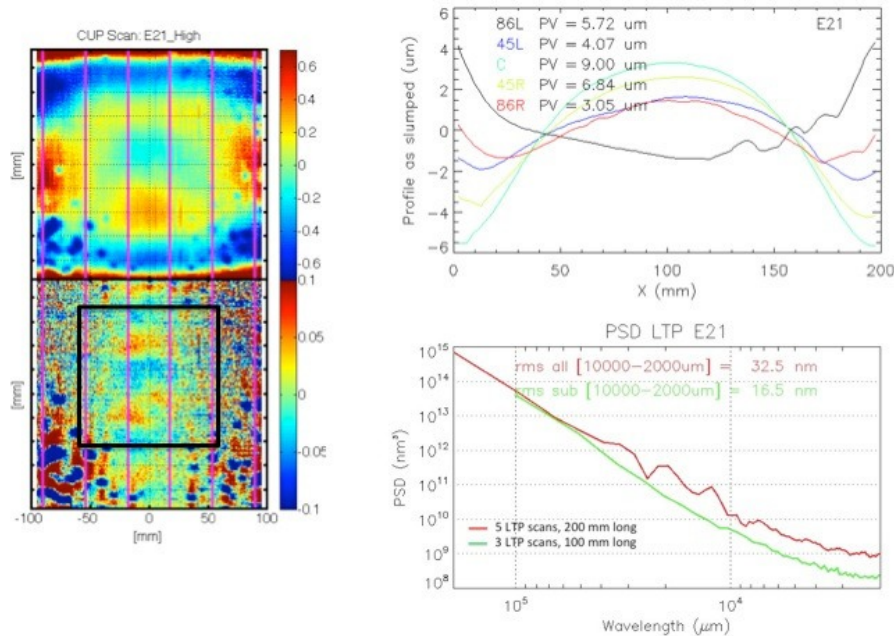

Figure 9. : *E21 measurements at INAF-OAB. Left: the residual of the CUP map after the subtraction of the cylinder of radius 1 m, and after removing the Legendre polynomials up to the 2nd order (top) or 8th order (bottom). Right: the five LTP scans (top) and the PSD (bottom) computed both from the five LTP scans (red curve), of length 200 mm, and the three LTP central scans (green curve) in the selected region of length 100 mm, giving rms(2 ÷10 mm) = 16.5 nm, computed without any detrend.*

The best area of size 100×100 mm² (black box in the CUP map of Fig. 9), the typical size for the SAO project, was selected out of the CUP map, excluding the area degraded by the contaminations. In order to compute the rms value in the spatial wavelength range $1 \div 10$ mm, LTP scans were used, as LTP is more accurate than CUP in this wavelength range. Five LTP scans, of length 200 mm and distance of about 40 mm from each other, were used to compute the PSD of the 200×200 mm² foil. The three inner ones, with length of 100 mm, were used to compute the PSD of the 100×100 mm² subsection delimited by the black box. Actually, the step size used for the LTP was 1 mm, therefore the minimum measured spatial wavelength is 2 mm. In the 100×100 mm² area, the rms $(2 \div 10$ mm) turned out as high as 16.5 nm, when computed without any detrend. Anyway, the rms from the WYKO measurements on E21, in the spatial wavelength 2.5 mm $\div 10$ μm was 1.3 nm, suggesting that the LTP rms in the millimetre range was affected by the sag error of the glass foil. In fact, the Fourier contribution of a polynomial is spread over all spatial wavelengths. Therefore, a low frequency error in the slumped glass foil would not contribute to the PSD in the millimetre spatial range only in case of a sinusoidal error, whereas it would contribute in case of polynomial errors.

As a cross check, E21 was measured at SAO on the WFS mounted on their optical profilometer. Since, at the time of the measurement, only the setup for flat glass foils was available, a limited portion of glass could be sampled in each measurement. The result was rms(1-10 mm) $\sim$ 2-3 nm in the selected 100 $\times$ 100 mm^2 glass sub region, within the instrumental noise. The result of this cross check was the acceptance of our hot slumped foils for the pre-determined figure correction test. Anyway, it appears that it was necessary to cast more light on how to correctly compute the mid-frequency errors.

3.2 Second test for mid-frequency error determination

In order to better understand the quality of our slumped glass foils in the 1 $\div$10 mm range, another glass foil (code E32) was characterised at INAF-OAB, after the delivery of the E21 foil to SAO. Actually, this foil was slumped on a K20 mould with poorer surface quality, as at that time the better one was at a re-polishing step. The exercise was anyway intended to understand the disagreement in the LTP and WYKO PSDs observed for each of our foils, as well as for the E32 one, as shown in Fig. 10-left: the PSD of the LTP measurement is the blue line in the wavelength range 2 $\div$200 mm (the typical step size we use is 1 mm), the PSD of the WYKO measurement is the green line in the wavelength wavelength range 10 $\div$2600 μm. The usual detrend for the WYKO data foresees to remove the 2nd order best fit polynomial (which is affected by the curvature of the optical system used for the measurements) and sometimes, as we do, the 4th order best fit polynomial to correct for misalignment of the sample during the measurement. No big difference is observed in the overall roughness PSD when removing the 2nd or the 4th polynomials. For the LTP data, the first approach was to remove only a first order polynomial. Anyway in this way, the two curve do not connect with each other (Fig. 10-left). This is due to the fact that the polynomials, present in the LTP profile measurements, have Fourier components in all frequency ranges, while, for the WYKO, the short scans are not affected by a polynomial curvature.

In order to connect the LTP and WYKO PSD (Fig. 10-right), only the central scan with length of 100 mm was considered, and the measurement was performed with a 0.1 mm step size (red dotted line). The decreased step size actually does not change the result, but enables the computation of the PSD down to 0.2 mm instead than 2 mm. In order to connect the shape and roughness PSDs curves, a 4th order best fit polynomial must be removed (red solid line) from the LTP profile. From this last curve, we have evaluated the contribution of the mid- frequency errors in the range 2 $\div$10 mm, giving an rms of 3.1 nm. This number should be considered as an upper limit, as this foil was slumped on a poorer K20 mould; the same analysis should be repeated in future, on the most recent process developed on a K20 with good surface quality.
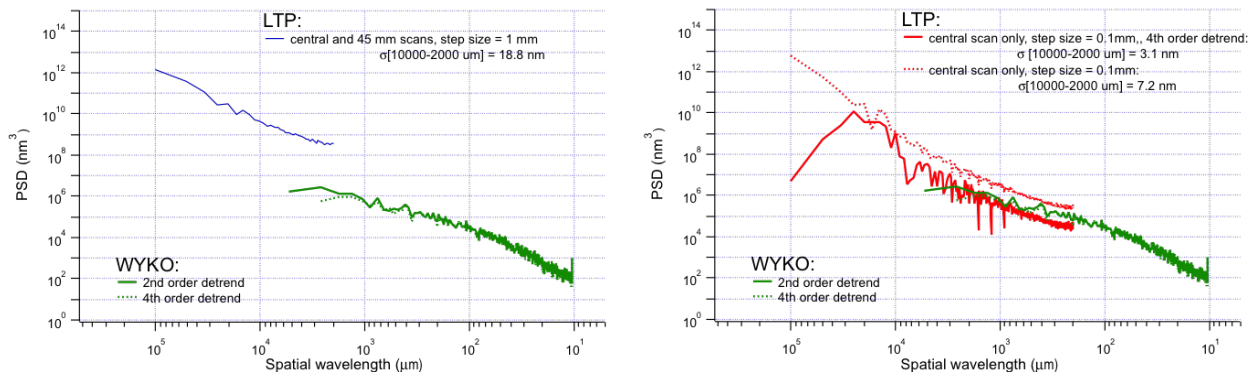

Figure 10. : *PSD from LTP and WYKO data, for the glass foil E32. Left: the PSD from five LTP scans of length 200 $\times$ 200 mm^2 is computed after removing only a first order polynomial (blue line), while the PSD from the WYKO data are computed after removing both the 2nd (green solid line) and the 4th order (green dotted line) best fit polynomial. In this case the two PSDs do not superimpose. Right: the PSDs from the central scan only is considered. The LTP scan was measured with a step size of 0.1 mm and produced a PSD line (red dotted line) still higher than the WYKO PSD if only a first order polynomial is removed from the LTP data. When a 4th order best fit polynomial is removed from the LTP scan, the corresponding PSD (red solid line) finally matches the roughness PSD. In this case rms[2 $\div$10 mm] = 3.1 nm.*

4. CUTTING FROM 200 × 200 mm² TO 100 × 100 mm².

Slumped glass foils are produced at INAF-OAB with an initial size of 340 × 340 mm². They are then trimmed to the size of 200 × 200 mm². Due to process constrains in the deposition of the piezo-electric elements, the size required by SAO is 100 × 100 mm². Preliminary measurements performed on our slumped glass foils, after cutting them to 100 × 100 mm² with the Penett MDI tool, returned the indication of shape modification after cutting. It is not clear, at the moment, whether the shape modification is induced by the cutting process or by the release of internal stresses in the slumped glass foil.

4.1 The cutting of a curved glass foil

The cutting of the cylindrically slumped glass foils is performed, in our laboratories, with the MDI patented scribing wheel (Penett®) which creates a groove up to 90% on the glass thickness (Fig. 11-left). A preliminary cut is performed from 340 × 340 mm² to the size of approximately 230 × 230 mm², over a convex cylindrical cutting mandrel of size 250 × 250 mm². After that, the glass, positioned on the cutting mandrel, can be clamped on a cylindrical template (Fig. 11-right), and cut to the size of 200 × 200 mm², or lower.
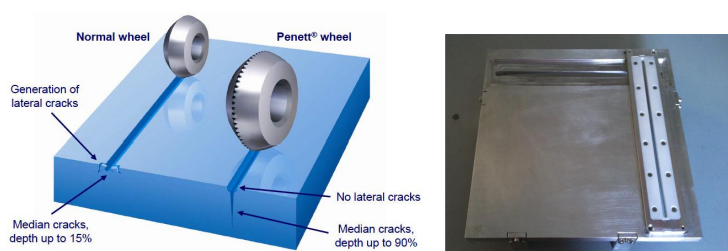

Figure 11. : *Left: the MDI Pennet's wheel, credits: MDI. Right: the template used at INAF-OAB to cut the slumped glass foils: the template has a bottom surface cylindrically shaped to follow the cylindrical cutting mandrel.*

4.2 Shape modification

In order to characterize the shape change with the cutting, two slumped glass foils (glass code E46 and E56, Fig. 4, 5) were measured after a progressive cut from 200 × 200 mm² to 100 × 100 mm². The shape profiles of these glass foils after slumping were very different (Fig. 12), due to the different pressure conditions during the slumping process (Figs. 4 and 5).

Two different metrology instruments were used for the characterisation:

1. mono dimensional profiles:

   the CHRocodile optical sensor 3300 μm, mounted on our LTP head, measures distances in the range of 3.3 mm with a 100 nm vertical resolution and 6 μm lateral resolution. It is operated in "thickness" configuration, to enable the measurement on both glass surfaces. The glass is supported on three bearing points and measured on both concavity. The actual profile of the optical side of the glass is retrieved by subtracting the two scans: this enables removing both gravity and bearing points deformations. A Rodenstock RM600-S sensor is also installed to subtract, in real time, the LTP stage error contribution by measuring a calibrated rod.

   For the size of 200 × 200 mm², a comparison was performed also with the pure LTP measurements after the subtraction of the deformation obtained by FEA. Actually this last method is less accurate in the low-frequency range as it includes FEA deviations from the nominal, due for instance to cutting errors.

   The comparison of the E46 and E56 glass shape profiles measured by LTP and CHR at different sizes are shown in Figs. 12, 13, 14. The measurements were carried out along three positions: at the central scan and at 45 mm off the central scan, both in left and right directions. The observed change in glass shape is in the same direction in each measured line; in particular, the central scan reverses its concavity, going concave upwards.

2. bi-dimensional maps:

the CUP[29] operated in our laboratories was used for the 2D characterisation. A CHRocodile optical sensor 660 μm (20 nm vertical resolution and 2 μm lateral resolution) is used as a null sensor, while a SIOS triple beam interferometer measures the distance from a reference mirror. The glass is vertically positioned in front of the CHR sensor. Fig. 15 shows the CUP maps of E46 and E56 at different sizes. The first raw shows the map after the subtraction of the cylinder. The second and third ones, give the maps after the subtraction of the Legendre polynomials up to the 2nd and 8th order respectively, to evidence mid-frequency errors.
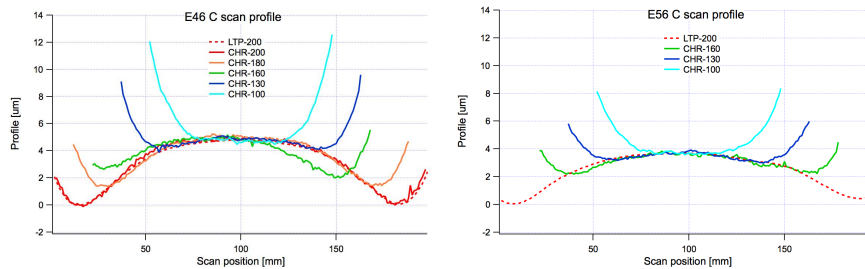

Figure 12. : *Profile changes after cutting at different size for the central scan, for E46 (left) and E56 (right).*
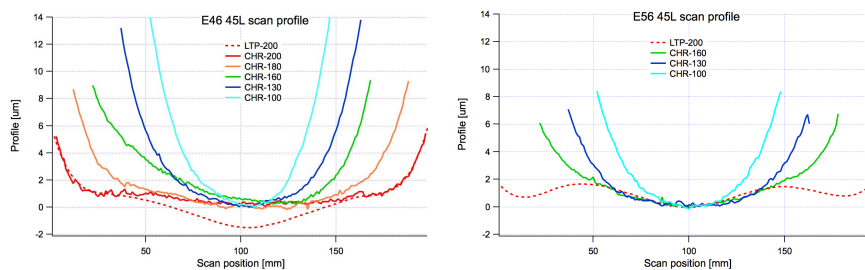

Figure 13. : *Profile changes after cutting at different size for the scan 45 mm left from the central one, for E46 (left) and E56 (right).*
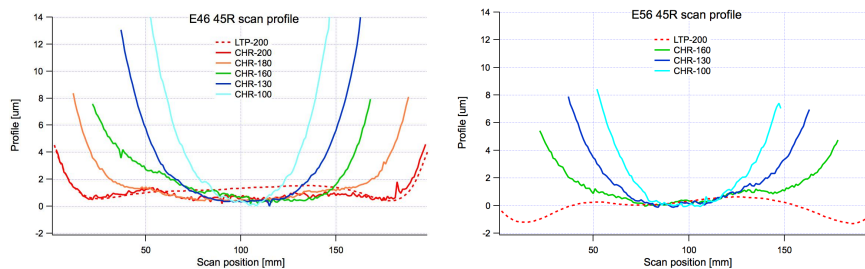

Figure 14. : *Profile changes after cutting at different size for the scan 45 mm right from the central one, for E46 (left) and E56 (right).*

The CHR, LTP and CUP results are fully consistent. In particular we can conclude that:

- from the first raw maps of Fig. 15, we see that, despite the different initial shape (pronounced deformation at the foil cornes for E46, while more homogeneous map for E56) the trend upon cutting is very similar;
- from the third raw maps of Fig. 15, we note that the mid frequency errors after cutting to 100 × 100 mm^2 are very similar for E46 and E56, while they are apparently different at size of 200 × 200 mm^2. This support the fact that to evaluate the mid frequency errors, we need to perform a detrend on a smaller size parts, in order to remove the effects of polynomials, as shown in Section 3.2.
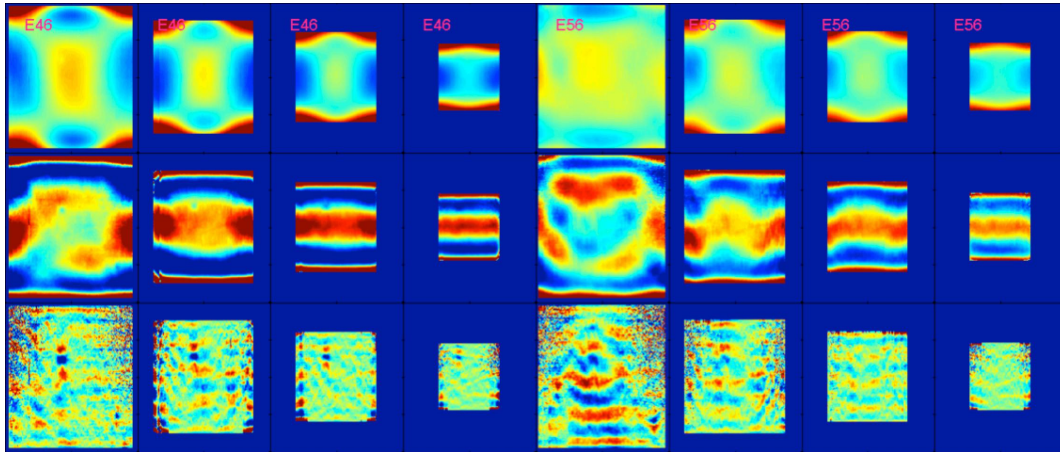
Figure 15. : *Shape variation of E46 and E56 glass foils, as measured by the CUP at sizes of 200 - 160 - 130 - 100 mm. Top: linear residuals from profiles along the optical axis (color scale PV: 8 μm). Center: residuals after removing the Legendre polynomials up to the 2nd order (Color scale PV: 1.2 μm). Bottom: residuals after removing the Legendre polynomials up to the 8th order (Color scale PV: 0.2 μm). The glass foils cut to $100 \times 100 \ mm^2$ show a very similar mid-frequency pattern, consistent with the replication of the K20 pattern.*

5. CONCLUSIONS

In this paper, we have shown the effort done at INAF-OAB to improve the optical quality of our slumped glass foils for active optics purposes in the X band. A continuos improvement in the hot slumping process at INAF-OAB was already proven in previous works. In this paper we have described in details some of the optimisation carried out recently. Several hardware modifications are presented: a closed cover for the muffle to reduce the thermal gradients in the slumping environment; the implementation of temperature recording at the slumping mould level inside the muffle; the implementation of the pressure value recording. Also software optimisation were implemented: different pressure control systems were tested and the application of pressure in open loop was defined as the best for reproducibility and quality results, specially in terms of mid-frequency errors; a new thermal cycle was implemented to reduce the high-frequency errors in the slumped glass foils.

Some of the slumped glass foils were used by the italian AXYOM project, which adopts both ribs and active piezo elements (glued on the back side) for the correction of the shape errors, and for tests performed for the american X-ray Surveyor mission, in particular for the deterministic figure correction of curved foils performed at SAO on our slumped foils, where the active piezo elements were sputtered and lithographically patterned on the back side at PSU.

The more stringent requirement of the X-ray Surveyor were considered as reference for our slumped foils: the high frequency errors (not correctable with the active approach) have been reduced from about 21 to 6-7 Å, compared to a requirement of 3.6 Å. To further improve the result, the Zerodur K20 surface should be polished to lower roughness. For the mid-frequency errors, the critical range is the 1 ÷10 mm, as this cannot be corrected by the active approach. For this value, we have given an upper limit of 3.1 nn rms, compared to the requirement of 1 nm: this was obtained with an exercise performed on a glass slumped on K20 with poor quality. The same test should be repeated on a foil slumped on the high quality K20 mould, with the newly developed slumping process. Finally for the low frequency range, no strict requirement was given nor by the X-ray Surveyor test of deterministic figure correction, or by the AXYOM project where also ribs are used to correct for low frequency errors. In the low-frequency range, we have experienced a profile change upon cutting from $200 \times 200 \ mm^2$ to $100 \times 100 \ mm^2$, necessary for the present configuration of the PSU coating equipment. Two foils were fully characterised upon cutting, showing a similar behaviour despite the different starting shape. To cast some light on this shape change, repeatability tests should be performed and different cutting tools should be tested. Finally, similar mid-frequency errors for these two

foils are observed at the size of $100 \times 100 \text{ mm}^2$ after removing the Legendre polynomial up to the 8th order: this is consistent with the procedure adopted in this paper to evaluate the mid-frequency errors, obtained by removing the low frequency polynomial contributions in the Fourier components around the region of interest for the mid-frequency.

ACKNOWLEDGMENTS

REFERENCES

[1] Spiga, D., Barbera, M., Collura, A., Basso, S., Candia, R., Civitani, M., Di Bella, M., Di Cicca, G., Lo Cicero, U., Lullo, G:, Pellicciari, C., Riva, M., Salmaso, B., Sciortino, L., Varisco, S., "Manufacturing an active X-ray mirror prototype in thin glass", Journal of Synchrotron Radiation, Vol 23, Issue 1 (2016)

[2] Spiga, D., Barbera, M., Collura, A., Basso, S., Candia, R., Civitani, M., Di Cicca, G., Lo Cicero, U., Lullo, G., Pellicciari, C., Riva, M., Salmaso, B., Sciortino, L., Varisco, S., "Realization and drive tests of an active thin glass x-ray mirror", Proc. SPIE 9965, this conference (2016)

[3] Civitani, M., Basso, S., Citterio, O., Conconi, P., Ghigo, G., Pareschi, G., Proserpio, L., Salmaso, B., Sironi, G., Spiga, D., Tagliaferri, G., Zambra, A., Martelli, F., Parodi, G., Fumi, P., Gallieni, D., Tintori, M., Bavdaz, M., Wille, E.: "Accurate integration of segmented X-ray optics using interfacing ribs", Optical engineering 52, (9), 091809 (2013)

[4] Spiga, D., Basso, S., Bavdaz, M., Burwitz, V., Civitani, M., Citterio, O., Ghigo, M., Hartner, G., Menz, B., Pareschi, G., Proserpio, L., Salmaso, B., Tagliaferri, G., Wille, E., "Profile reconstruction of grazing-incidence x-ray mirrors from intra-focal x-ray full imaging", Proc. SPIE 8861, 88611F (2013)

[5] Lo Cicero, U., Sciortino, L., Lullo, G., Di Bella, M., Barbera, B., Collura, A., Candia, R., Spiga, D., Basso, S., Civitani, M., Pelliciari, C., Salmaso, B., "Electrical connections and driving electronics for piezo-actuated x ray thin glass optics", Proc. SPIE 9965, this conference (2016)

[6] Gaskin, J.A., et al., " The X-ray Surveyor mission: a concept study", Proc. SPIE 9601, 96010J (2015)

[7] Reid, P.B., Aldcroft, T.L., Allured, R., Cotroneo, V., Johnson-Wilke, R.L., Marquez, V., et al., "Development status of adjustable grazing incidence optics for 0.5 arcsecond x-ray imaging", Proc. SPIE 9208, 920807 (2014)

[8] Ulmer, M. P., Wang, X., Cao, J., Savoie, J., Bellavia, B., Graham, M. E., Vaynman, S., "Progress report on using magneto-strictive sputtered thin films to modify the shape of a x-ray telescope mirror", Proc. SPIE 8503, 85030C (2012)

[9] Kilaru, K., Ramsey, B. D., Gubarev, m., Gregory, D., "Differential deposition technique for figure corrections in grazing-incidence x-ray optics", Opt. Eng., 50 (10), 106501 (2011)

[10] Chalifoux, B., Wright, G., Heilmann, R. K., Schattenburg, M. L., "Ion implantation for figure correction of thin x-ray telescope mirror substrates", Proc. SPIE 9603, 96031K (2015)

[11] Riveros, R. E., et al., "Progress on the fabrication of high resolution and lightweight monocrystalline silicon X-ray mirrors", Proc. SPIE 9905, in press (2016)

[12] Gubarev, M.V., et al., " Development of the a direct fabrication technique for full-shell x-ray optics", Proc. SPIE 9905, in press (2016).

[13] Pareschi, G., et al., "Beyond Chandra: problems, solutions, and perspectives for the implementation of very high angular resolution x-ray telescopes in the new millennium", Proc. SPIE 9905, in press (2016).

[14] Reid, P. B., Cameron, R. A., Cohen, L., Elvis, M., Gorenstein, P., Jerius, D., Petre, R., Podgorski, W. A., Schwartz, D. A., Zhang, W. W., "Constellation-X to Generation-X: evolution of large collecting area moderate resolution grazing incidence x-ray telescopes to larger area high-resolution adjustable optic", Proc. SPIE 5488, 325-334 (2004)

[15] O'Dell, S. L., Atkins, C., Button, T. W., Cotroneo, V., Davis, W. N., Doel, P., Feldman, C. H., Freeman, M. D., Gubarev, M. V., Kolodziejczak, J. J., Michette, A. G., Ramsey, B. D., Reid, P. B., Rodriguez Sanmartin, D., Saha, T. T., Schwartz, D. A., Trolier-McKinstry, S., Wilke, R. H. T., Willingale, R., Zhang, W. W., "Toward active x- ray telescopes", Proc. SPIE 8147, 1Q 14pp (2011)

[16] Vikhlinin, A., Reid, P., Tananbaum, H., Schwartz, D. A., Forman, W. R., Jones, C., Bookbinder, J., Cotroneo, V., Trolier-McKinstry, S., Burrows, D., Bautz, M. W., Heilmann, R., Davis, J., Bandler, S. R., Weisskopf, M. C., Murray, S. S., "SMART-X: Square Meter Arcsecond Resolution x-ray Telescope", Proc. SPIE 8443, 16 12pp (2012)

[17] Wilke, R. H. T., Johnson-Wilke, R. L., Cotroneo, V., Davis, W. N., Reid, P. B., Schwartz, D. A., Trolier- McKinstry, S., "Sputter deposition of PZT piezoelectric films on thin glass substrates for adjustable x-ray optics", Appl. Opt. 52, 3412-3419 (2013).

[18] Cotroneo, V., Davis, W.N., Reid, P.B., Schwartz, D., Trolier-McKinstry, S., Wilke, R.H.T, "Adjustable grazing incidence x-ray optics: measurement of actuator influence functions and comparison with modeling", Proc. SPIE 8147, 81471R-1 (2011)

[19] Proserpio, L., Civitani, M., Ghigo, M., Pareschi, G., "Thermal shaping of thin glass substrates for segmented grazing incidence active optics", Proc. SPIE 7803, 78030K-2 (2010)

[20] Salmaso, B., Brizzolari, C., Basso, S., Civitani, M.M., Ghigo, M., Pareschi, G., Spiga, D., Tagliaferri, G., Vecchi, G., "Slumped Glass Optics for X-ray telescopes: advances in the hot slumping assisted by pressure", Proc. SPIE 9603, 96030O (2015)

[21] Allured, R., Hertz, E., Marquez, V., Cotroneo, V., Wallace, M.L, Salmaso, B., Civitani, M., Trolier-McKinstry, S., Alexey, V., Pareschi, G:, Reid, P., " Laboratory demonstration of the piezoelectric figure correction of a cylindrical slumped glass optic", Proc. SPIE 9905 (2016)

[22] Allured, R., Ben-Ami, S., Cotroneo, V., Marquez, V., McMuldroch, S., Reid, P. B., Schwartz, D. A., Trolier-McKinstry, S., Vikhlinin, A. A., Wallace, M.L., " Improved control and characterization of adjustable x-ray optics", Proc. SPIE 9603, 96031M (2015)

[23] Proserpio, L., "Development of the glass slumping technology for the production of the x-ray mirrors aboard the International X-ray Observatory optical module", Ph.D. thesis (2011)

[24] Salmaso, B., Basso, S., Civitani, M.M., Ghigo, M., Holysko, J., Spiga, D., Vecchi, G., Pareschi, G., "Slumped Glass Optics development with pressure assistance", Proc. SPIE 9905, in press (2016)

[25] Salmaso, B., Brizzolari, C., Spiga, D., "A model supporting the use of pressure in the hot slumping of glass substrates for X-ray telescopes", Optics Express, submitted (2016)

[26] Salmaso, B., Basso, S., Brizzolari, C., Civitani, M.M., Ghigo, M., Pareschi, G., et al., "Production of thin glass mirrors by hot slumping for X-ray telescopes: present process and ongoing development", Proc. SPIE 9151, 91512W (2014)

[27] Salmaso, B., Basso, S., Brizzolari, C., Civitani, M., Ghigo, M., Pareschi, G., Spiga, D., Tagliaferri, G., Vecchi, G., "Direct hot slumping of thin glass foils for future generation X-ray telescopes: current state of the art and future outlooks", Proc. ICSO, (2014)

[28] Raimondi, L., Spiga, D., "Mirror for X-ray telescopes: Fresnel diffraction-based computation of point spread functions from metrology", AA 573, A22 (2015)

[29] Civitani, M.M., Ghigo, M., Citterio, O. Conconi, P. Spiga, D. Pareschi, G. Proserpio, L., "3D characterization of thin glass x-ray mirrors via optical profilometry", Proc. SPIE 7803, 78030L (2010)